Clinkenbeard Erica L (Orcid ID: 0000-0001-6687-1106)
Robling Alexander G (Orcid ID: 0000-0002-3989-4780)
Holguin Nilsson (Orcid ID: 0000-0001-8446-845X)

Suppression of sost/sclerostin and dikkopf-1 augment intervertebral disc structure in mice

Tori Kroon M.S.[1]
Neharika Bhadouria, M.S.[2]
Paul Niziolek, M.D., PhD.[3]
Daniel Edwards III[4]
Erica L Clinkenbeard, Ph.D.[4]
Alexander Robling, Ph.D.[4,5]
Nilsson Holguin, Ph.D.[4-6]

Keywords: Anabolic therapeutics, Chondrocyte and cartilage biology, Genetic animal models, Preclinical Studies, Wnt/β-catenin/LRPs

[1]Department of Biomedical Engineering, IUPUI, Indianapolis, IN, USA
[2]Department of Mechanical Engineering, Purdue University, West Lafayette, IN, USA
[3]Radiology & Imaging Sciences, IUPUI, Indianapolis, IN, USA
[4]Indiana Center of Musculoskeletal Health, Indianapolis, IN, USA
[5]Department for Anatomy and Cell Biology, IUPUI, Indianapolis, IN, USA
[6]Department of Mechanical and Energy Engineering, IUPUI, Indianapolis, IN, USA

Correspondence to:

Nilsson Holguin, Ph.D.
Assistant Professor
Department of Mechanical and Energy Engineering, IUPUI, 723 W. Michigan St,
Indiana Center of Musculoskeletal Health, IUPUI, 635 Barnhill Drive.
Indianapolis, IN, 46202, USA

Voice: 317-278-2642

Email: nholguin@iupui.edu

Tori Kroon: tkroon@iu.edu
Neharika Bhadouria: nbhadour@iu.edu
Paul Niziolek: pniziole@iupui.edu
Daniel Edwards III: dfedward@iu.edu
Erica L Clinkenbeard: eclinken@iu.edu
Alexander Robling: arobling@iupui.edu

Disclosure:

Competing Interests: No competing interests declared.

Data is available upon request.

This is the author's manuscript of the article published in final edited form as:

Kroon, T., Bhadouria, N., Niziolek, P., Edwards, D., Clinkenbeard, E. L., Robling, A., & Holguin, N. (2022). Suppression of sost/sclerostin and dikkopf-1 augment intervertebral disc structure in mice. Journal of Bone and Mineral Research. https://doi.org/10.1002/jbmr.4546

Abbreviations

μCT – micro-computed tomography

ACAN - Aggrecan

AF – Annulus fibrosus

BGLAP – Osteocalcin

BMD – Bone mineral density

BV/TV – Bone volume/tissue volume

COLI – Collagen type 1

COLII – Collagen type 2

COLX – Collagen type 10

DKK1 – Dickkopf WNT signaling pathway inhibitor 1

ECM – Extracellular matrix

FOXA2 – Forkhead box a2

GDF5 – Growth differential factor 5

IHC – Immunohistochemistry

IVD - Intervertebral disc

KO - Knockout

LRP – Low-density lipoprotein receptor-related protein

MRI – Magnetic Resonance Imaging

NP – Nucleus pulposus

qPCR - quantitative Polymerase Chain Reaction

Sclerostin – Protein product of Sost

sFRP4 – Selected frizzled-related protein 4

SP7/OSX – Osterix

Tb.N – Trabecular number

Tb.Th. – Trabecular thickness

WNT – Wingless-related integration site

WT – Wild-type

Abstract. Intervertebral disc (IVD) degeneration is a leading cause of low back pain, characterized by accelerated extracellular matrix breakdown and IVD height loss but there is no approved pharmacological therapeutic. Deletion of Wnt ligand competitor Lrp5 induces IVD degeneration, suggesting that Wnt signaling is essential for IVD homeostasis. Therefore, the IVD may respond to neutralization of Wnt ligand competitors *sost*(gene)/sclerostin(protein) and/or dikkopf-1 (dkk1). Anti-sclerostin antibody (scl-Ab) is an FDA-approved bone therapeutic that activates Wnt signaling. We (1) determined if pharmacological neutralization of sclerostin, dkk1 or their combination would stimulate Wnt signaling and augment IVD structure and (2) determined the prolonged adaptation of the IVD to global, persistent deletion of *sost*. Nine-week-old C57Bl/6J female mice (n=6-7/grp) were subcutaneously injected 2x/wk for 5.5 wk with scl-Ab (25 mg/kg), dkk1-Ab (25 mg/kg), 3:1 scl-Ab/dkk1-Ab (18.75:6.25 mg/kg) or vehicle (veh). Separately, IVD of *sost* KO and wildtype (WT) mice (n=8/grp) were harvested at 16 weeks of age. First, compared to vehicle, injection of scl-Ab, dkk1-Ab and 3:1 scl-Ab/dkk1-Ab similarly increased lumbar IVD height and β-catenin gene expression. Despite these similarities, only injection of scl-Ab alone strengthened IVD mechanical properties and decreased heat shock protein gene expressions. Genetically and compared to WT, *sost* KO enlarged IVD height, increased proteoglycan staining and imbibed IVD hydration. Notably, persistent deletion of *sost* was compensated by upregulation of *dkk1,* which consequently reduced the cell nuclear fraction for Wnt signaling co-transcription factor β-catenin in the IVD. Lastly, RNA-sequencing pathway analysis confirmed the compensatory suppression of Wnt signaling and revealed a reduction of cellular stress-related pathways. Together, suppression of sost/sclerostin or dkk1 each augmented IVD structure by stimulating Wnt signaling, but scl-Ab outperformed dkk1-Ab in strengthening the IVD.

Ultimately, postmenopausal women prescribed scl-Ab injections to prevent vertebral fracture may also benefit from a restoration of IVD height and health.

Keywords: Anabolic therapeutics, Chondrocyte and cartilage biology, Genetic animal models, Preclinical Studies, Wnt/β-catenin/LRPs

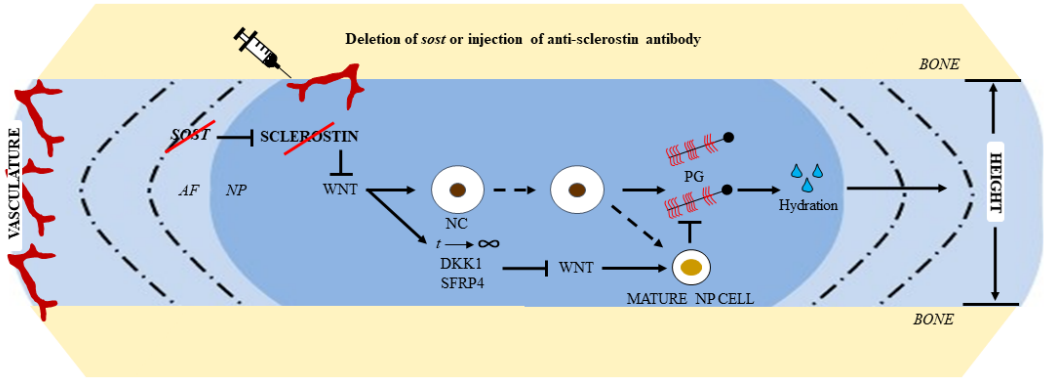

Graphical abstract: Suppression of Wnt signaling inhibitors by genetic or pharmacological approaches promoted intervertebral disc structure, strength, and hydration. However, persistent activation of Wnt signaling induced a compensatory upregulation of other Wnt signaling inhibitors that shifted IVD cells toward a mature NP cell phenotype. AF: annulus fibrosus, NC: notochordal cell, NP: nucleus pulposus, PG: proteoglycan

Introduction

There are no FDA-approved pharmacological treatments for intervertebral disc (IVD) degeneration,[1,2] a major contributing factor of low back pain.[3,4] Osteoporosis may contribute to IVD degeneration[5] and some pharmacological treatments for bone maintenance target anabolic pathways innate to the IVD. Anti-sclerostin-antibody (scl-ab) treatment is an FDA-approved bone anabolic[6] for postmenopausal women at high-risk of vertebral fracture.[7] Sclerostin and dkk1 are inhibitors of the Wnt/β-catenin signaling pathway and global suppression of sclerostin by systemic injection of scl-ab or genetic ablation of its precursor *SOST(human)/sost(mouse)* promotes bone formation and mildly attenuates bone resorption.[8] Individuals administered scl-ab do not report an altered incidence of back pain than control subjects, suggesting it might not be harmful to the IVD.[6] While osteocytes in bone are the major source of sclerostin[9,10] and dkk1,[11] IVD cells also express sclerostin and dkk1,[12] but the impact of regulating sost/sclerostin or dkk1 on the IVD has yet to be determined.

Sclerostin and dkk1 are inhibitors of the canonical Wnt signaling pathway but differ in some notable ways. Both dkk1 and sclerostin interact with LRP5/6 to competitively prevent various Wnt ligands from binding to initiate the canonical Wnt signaling pathway.[11] β-catenin is a key co-transcription factor in the Wnt signaling pathway, where activation of this pathway is comprised of β-catenin translocation to the cell nucleus, association with co-transcription factors TCF and LEF, and transcription of target genes.[13] Wnt/β-catenin signaling regulates cell fate and extracellular matrix (ECM) anabolism in a range of musculoskeletal tissues. For instance, inactivation of Wnt signaling shifts differentiation of mesenchymal stem cells from osteoblastogenesis to chondrogenesis[14] and activation in early chondrocytes triggers

hyperchondrocyte maturation.[15] Sclerostin and dkk1 can both bind to the first β-propeller of LRP5/6, but dkk1 can also bind to the second, third and fourth β-propellers of LRP5/6[16,17,18] A pathway-related distinction between dkk1 and sclerostin is that dkk1 is a direct target of Wnt/β-catenin signaling pathway.[19]

In the spine, IVD development requires Wnt signaling,[20] and loss of Wnt signaling by aging and/or injury[21,22] blunts ECM anabolism.[12,21] The nucleus pulposus serves as the hydration core of the IVD and houses notochordal cells that require Wnt signaling to maintain their cellular phenotype.[23] Age- and injury-related reduction of Wnt signaling trigger the replacement of notochordal cells by more mature nucleus pulposus cells that are less equipped to produce ECM.[21,24] Contrarily, genetic stabilization of β-catenin in the nucleus pulposus increases notochordal cell expression and ECM anabolism[24] and can promote ECM-related transcription during IVD injury.[12] Lastly, in vivo deletion of LRP5 in IVD cells reduces Wnt signaling[21] and suggests that the IVD may be sensitive to Wnt ligand competitors that bind LRP5/6.

Therefore, we hypothesized that (1) neutralization of sclerostin and/or dkk1 and (2) deletion of gene precursor to sclerostin *sost* would stimulate ECM anabolism in the IVD by increasing canonical Wnt signaling. Neutralization of sclerostin, dkk1 and in combination similarly increased Wnt signaling and IVD height. Next, using histology, MRI, qPCR and RNA sequencing, global genetic deletion of *sost* increased the water content of the IVD, proteoglycan staining, IVD height and decreased cellular stress mechanisms related to protein folding, but these changes were accompanied by gene and protein expression changes consistent with mature cell phenotypes by

compensation of Wnt signaling. Overall, suppression of *sost*/sclerostin and/or dkk1 augment the structure of the IVD.

Methods and Materials

Mice

(1) 9-week-old C57Bl/6J female mice (n=6-7/group) were injected with 25 mg/kg of either anti-sclerostin antibody (scl-Ab), anti-dkk1 antibody (dkk1-Ab), a 3:1 ratio of the two antibodies (18.75 mg/kg of scl-Ab and 6.25 mg/kg of dkk1-Ab), a 1:1 ratio (12.5 mg/kg of scl-Ab and dkk1-Ab), a 1:3 ratio (6.25 mg/kg of scl-Ab and 18.75 mg/kg of dkk1-Ab), or the buffer in which the antibodies were made (veh) for 5.5 weeks, twice per week (all previously described,[25, 26] see Table 1). L3-S1 of these mice were used for another study and not analyzed here. (2) *Sost* KO mice and their wild-type (WT) littermates (n=8/group total) on a C57Bl/6 background have been previously described.[25] Mice were housed in a 12-hour light/dark cycle, fed standard chow, and all experiments were performed with prior IACUC approval. Lumbar and caudal (tail) spinal sections were harvested. Mice were euthanized by hypoxia as a primary means and cervical dislocation as a secondary means. Spinal levels were further divvied-up for specific testing (Table 2).

Table 1. Scl-Ab and/or dkk1-Ab dosage

Group	Scl-Ab (mg/kg)	Dkk1-Ab (mg/kg)	Total Ab (mg/kg)	n
Veh	0	0	0	7
Scl-Ab	25	0	25	6
Dkk1-Ab	0	25	25	7
3:1	18.75	6.25	25	7
1:1	12.5	12.5	25	7
1:3	6.25	18.75	25	7

N/A: Not applicable

Table 2. Functional spinal unit or bone for each outcome.

Outcome	Tail	Lumbar
MRI	CC6-7	N/A
Mechanics	CC6-7	N/A
Western Blot	CC6-8, CC10-12	N/A
μCT	CC7	L6
qPCR	CC8-10, CC4-5 and CC14-15	L3-5
Histology	CC11-13	L1-3

Note: CC4-5 and CC14-15 segments used for the injection-related groups. N/A: Not applicable

Histology and Immunohistochemistry

IVD for each stain were run in a single batch. L1-3 and CC10-11 were fixed in 15 mL of 10% formalin on a rocker for 24 hours, submerged in 70% ethanol, embedded in paraffin, and sectioned (5 μm). Safranin-O/fast-green counterstain images were analyzed by 4 independent observers for an average IVD degeneration score.[21,27] In short, the NP, AF and boundary between the two structures were scored based on structural properties and added for a total IVD score between 0-14, with increasing scores denoting greater IVD degeneration. Qualitatively, proteoglycan in the NP was estimated as the amount of intensity staining per area using ImageJ. Alcian blue staining was the counterstain for the IHC staining of sclerostin (BAF 1589, R&D Systems), osterix (#22552, Abcam), and collagen 2 (II-II6B3-c, DSHB). For both osterix and collagen 2 quantification in the NP, positive cells were counted and compared to the total number of cells that were stained brown for the protein and blue for the cell nuclei. The percent of the area-stained brown for osterix was quantified and compared for the AF. Samples with sectioning anomalies and statistical outliers (*see* Statistics) were excluded from analysis. Total sample size per group was noted in each figure description.

Mechanical Testing and Analysis

Following extraction of CC6-CC7 motion segments, the IVD was prepared, mechanically tested and analyzed based on a previously published technique (Liu et al. J Biomech 2015).[28] The IVD was isolated from vertebrae CC6 and CC7 by dissection at the growth plate with the assistance of a microscope (M400 Photomakroscop; Wild, Heerbrugg, Switzerland). Growth plate-IVD-growth plate segments were imaged by an X-ray machine (Bruker) to determine IVD height using ImageJ (NIH). Next, a petri dish was glued to each IVD using cyanoacrylate and filled with phosphate buffered saline (PBS, pH: 7.2) to maintain an osmotic environment. IVD were tested using a microindentation system (BioDent; Active Life Scientific, CA) for quasi-static and dynamic mechanical properties. The testing sample was aligned with a 2.39 mm probe that fully covered the entire IVD and loaded sinusoidally (1 Hz) for 20 cycles under a preload of 20 grams at a compressive strain of 5%. Compressive strains were determined using x-ray-derived IVD heights. Triplicate trials were performed at each strain, with at least 10 minutes of rest time between each trial.

MATLAB code was used to remove the noise generated from the first and last loading cycle in the force-distance curve for each trial. The mechanical property outcomes from a semi-automated software program included relative maximum force (N), displacement (μm), loading stiffness (N/μm), unloading stiffness (N/μm), energy dissipation (N·μm=μJ) and loss tangent from the force-distance curve. Relative maximum force and displacement were calculated by considering the difference between the maximum and minimum values for these outcomes. Each outcome was computed as the average of the two trials with the lowest standard deviation out of three trials.

Magnetic Resonance Imaging (MRI)

Motion segment CC6-7 was submerged and wrapped in 1x PBS-soaked gauze overnight until imaged. Imaging was completed on the Bruker BioSpin 9.4 T MRI, using a 400 nm slice thickness for 2D imaging. The motion segment was imaged in a sagittal orientation using a 0.052 x 0.052 mm voxel resolution in the x-y direction and a 0.4 mm voxel resolution in the z-direction taking 16 averages/slice. Two samples were stacked in a glass tube to remain upright, and two glass tubes were placed, separated by foam composite, inside of a 15mL tube to ensure samples would not move while being imaged. Images were analyzed for quantification by ImageJ (NIH). Area and intensity of the IVD were determined and multiplied to estimate the hydration content of the IVD.

Micro-Computed Tomography

Motion segments L6-S1 and CC6-7 were harvested and submerged in 1x PBS prior to imaging. Specimens were imaged using the Bruker SkyScan 1272 Micro-CT at a resolution of 8 micrometers. Vertebral bone was contoured at the periosteum and endosteum for trabecular and cortical analysis. For the trabecular analysis, the growth plate was used as a landmark and trabecular bone analysis consisted of the next 30 consecutive images (slices).[29] For cortical analysis, the longitudinal center of the bone was identified and 15 images above and below were analyzed using the Bruker CTan64 MicroCT software.[17] Parameters measured included BV/TV (bone volume/tissue volume), trabecular number (Tb.N), trabecular thickness (Tb.Th) for trabecular bone and cross-sectional thickness for cortical bone, using a lower threshold of 60 and upper threshold of 225 for analysis.

QPCR

L3-5 and CC8-10 IVDs were harvested, frozen in liquid nitrogen, pulverized and suspended in TRIZOL (Ambion) until further processing.[17] RNA isolation and purification steps were followed (RNeasy mini kit, Qaigen) and RNA concentration was quantified (Nanodrop). CDNA was synthesized (iScript, Biorad) from 400 ng of total RNA for the following Taqman probes (Life Technologies); *aggrecan* (Mm00565794_m1), *keratin8* (Mm04209403_g1), *dmp1* (Mm01208363_m1), *sost* (Mm00470479_m1), *adamts5* (Mm00478620_m1), *collagen1* (Mm00801666_g1), *collagen2* (Mm01309565_m1), *osterix* (Mm04209856_m1), *β-catenin* (Mm01350387_g1), *serpina1a* (Mm02748447_g1), *serpina1c*+ (Mm04207703_mH), *serpina1d* (Mm00842095_mH), *sostdc1* (Mm03024258_s1), *foxa2* (Mm01976556_s1), *axin2* (Mm00443610_m1), *sfrp4* (Mm00840104_m1), *gdf5* (Mm00433564_m), *hspa1b* (Mm03038954_s1), *cxcl9* (Mm00434946_m1), *il1b* (Mm00434228_m1), *wnt16* (Mm00446420_m1), *dkk1* (Mm00438422_m1), *Wnt3a* (Mm00437337_m1). Relative gene expression was normalized to *IPO8* (Mm01255158_m1) for each group and then experimental values (*sost* KO) were normalized to the average of the WT values ($2^{-\Delta\Delta CT}$).

Western Blotting

WT and *sost* KO IVDs between CC6-8 were isolated for whole cell lysate, and cytoplasmic and nuclear separation western blots.[30] IVDs were minced in ice-cold phosphate buffered saline (PBS; Fisher) containing 2% fetal bovine serum (FBS; Atlanta biologicals) and protease inhibitor PMSF (Sigma). Two tail IVDs from a single animal, per isolation method, were homogenized using a Tissue Tearor (BioSpec Products). Whole cell lysate was generated using diluted 1x cell lysis buffer (Cell Signaling) supplemented with PMSF. Fractionation of the nuclear protein was

performed according to the Pierce cytoplasmic and nuclear extraction kit instructions (Sigma). Samples were run on an SDS-Page gel (BioRad) and transferred to PVDF membrane (BioRad). Blots were probed for anti-β-catenin (unphosphorylated; Cell Signaling) and subsequently an HRP-tagged anti-rabbit secondary antibody (#7074S, Cell Signaling). Whole cell lysates were normalized to HRP-tagged actin antibody (#A3854, Sigma Aldrich) and nuclear fractions to HRP-tagged histone H3 (#12648, Cell Signaling). All blots were developed using Immobilon Luminata Forte (Sigma) and the images were digitally collected with the Amersham Imager 600 (GE Healthcare). Densitometry quantification was conducted on ImageJ to enumerate relative protein values between groups.

Bioinformatics

Gene Set Enrichment Analysis software, GSEA, was used to generate the top down- and up-regulated pathways by deletion of *sost* in the IVD. The input included gene name and raw counts for each sample. WEB-based Gene SeT AnaLysis Toolkit was used to generate the top up- and down-regulated pathways between the WT and *sost* KO group. Using GSEA method of interest and geneontology for the functional database, the input included gene symbols and associated fold change for each gene. R Studio was used to generate plots such as PCA plot, volcano plot and heat maps.

Statistics

Post ANOVA, a Dunnett's test was used for the injection-related studies, with vehicles as the main comparison. A one-sample t-test was used to test for outliers beyond 3 SD. A Student's t-test was used between WT and *sost* KO IVD and between Veh and Scl-Ab. Box plots were used as the

main graphical output. A box plot displays a 5-number summary of the data. The top and bottom lines of the box plot represent the first and third quartile while the center line in the box is the median. The top and bottom points represent the minimum and maximum of the data. Each point on the graph represents one sample. Total number of samples for each analysis are included in the figure legend. False discovery rate (FDR) was computed from p-values using the Benjamini-Hochberg procedure. A p-value or FDR-value (where applicable) < 0.05 was considered significant.

Results

Injection of neutralization for sclerostin, dkk1 and in 3:1 combination increased IVD height.

Preliminary data suggested that the IVD gene expression of *sost* relative to *dkk1* is ~3:1 (data not shown). Therefore, in addition to scl-Ab or dkk1-Ab, we injected mice at 3:1, 1:1, and 1:3 scl-Ab:dkk1-Ab for consistency. Systemic administration of scl-Ab, dkk1-Ab, and the 3:1 combination of scl-Ab and dkk1-Ab increased lumbar IVD height ($F=7.74$ and $p<0.001$) by 22%, 26%, and 32% ($p = 0.02, 0.02, 0.005$), respectively (Fig. 1A, B) but the 1:1 and 1:3 combination injections did not significantly increase IVD height. Neither IVD degeneration score nor proteoglycan staining intensity were altered by any injections. In tail IVD, no variety of injection impacted IVD height ($F=0.73$ and $p=0.60$), proteoglycan staining intensity ($F=3.88$ and $p=0.01$) or IVD degeneration score ($F=1.25$ and $p=0.31$) (Supplemental Figure 1).

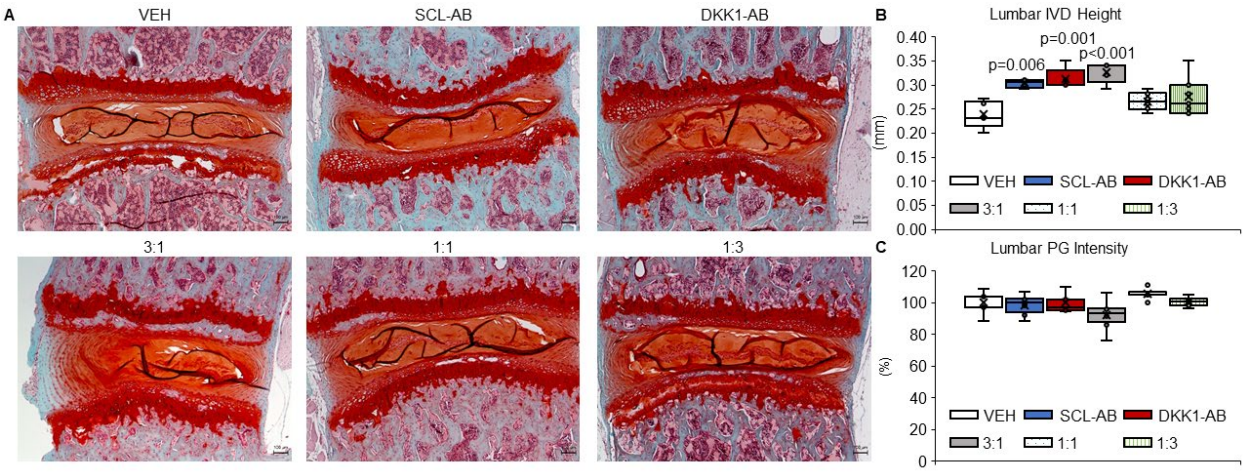

Figure 1. Quantitative and qualitative IVD structural properties. (A) 5X magnification images of Safranin-O and Fast Green counter stained histological sections of the lumbar IVD for vehicle (veh, n = 5 mice), 25 mg/kg anti-sclerostin-antibody injection (scl-Ab, n=5), 25 mg/kg injection of anti-dkk1-antibody (dkk1-Ab, n=5) (top row, left to right), combination injection of 18.75 mg/kg anti-sclerostin-antibody and 6.25 mg/kg anti-dkk1-antibody (3:1, n=5), combination of 12.5 mg/kg each of anti-sclerostin- and anti-dkk1-antibody (1:1, n=7), and a combination injection of 6.25 mg/kg of anti-sclerostin-antibody and 18.75 mg/kg of anti-dkk1-antibody (1:3, n=6) (bottom row, left to right). (B) Quantitative measurement of lumbar IVD height of all 6 groups. (C) Quantitative measurement of proteoglycan intensity staining in percentage of the lumbar IVD. Red staining for proteoglycan. Scale bar is 100 μm. Injection groups were compared to the vehicle group using a Dunnett's test, with significance noted below $p<0.05$.

Injection of sclerostin-neutralization antibody improved IVD mechanics.

Despite no change in tail IVD height by injection of any Wnt signaling inhibitor neutralization combination compared to vehicle injection, injection of scl-Ab alone most improved the mechanical properties of tail IVD. Namely, injection of scl-Ab doubled ($p=0.006$, $p=0.008$, respectively) the loading ($F=2.52$ and $p=0.05$) and unloading stiffness ($F=2.76$ and $p=0.04$) of the

IVD. A similar trend appeared with ultimate force but no changes were statistically significant (F=1.35 and p=0.27). Neither energy dissipation, displacement nor loss tangent was affected by any injection group (F=3.44, 1.62, 1.59 and p=0.01, 0.18, 0.19).

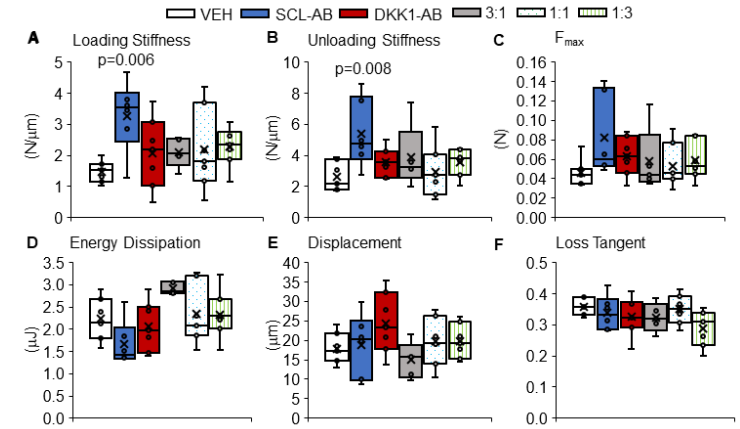

Figure 2. Injection of scl-Ab improved IVD mechanical properties. C57Bl6 mice were injected with vehicle (veh, n = 7 mice), 25 mg/kg anti-sclerostin-antibody injection (scl-Ab, n=6), 25 mg/kg injection of anti-dkk1-antibody (dkk1-Ab, n=7), combination injection of 18.75 mg/kg anti-sclerostin-antibody and 6.25 mg/kg anti-dkk1-antibody (3:1, n=6), combination of 12.5 mg/kg each of anti-sclerostin- and anti-dkk1-antibody (1:1, n=7), or a combination injection of 6.25 mg/kg of anti-sclerostin-antibody and 18.75 mg/kg of anti-dkk1-antibody (1:3, n=7). (A) Loading stiffness, (B) unloading stiffness, (C) ultimate force, (D) energy dissipation, (E) displacement and (F) loss tangent of the IVD. Injection groups were compared to the vehicle group using a Dunnett's test, with significance noted below $p<0.05$.

Injection of sclerostin-neutralization-, dkk1-, and 3:1 combinatorial-antibody stimulated Wnt signaling.

Quantitative PCR was determined in the injection groups that increased IVD height relative to vehicle: scl-Ab, dkk1-Ab and 3:1 scl-Ab:dkk1-Ab. Scl-Ab and dkk1-Ab upregulated transcription of canonical Wnt signaling co-factor *β-catenin* (F=4.346 and p=0.01) by 1.7-fold (p=0.04) and 1.2-fold (p=0.02), respectively (Fig. 3A). Injection of the 3:1 combination trended to upregulate *β-catenin* expression. Corroboratively, scl-Ab reduced *sost* gene expression by 85% (p=0.0004) and 3:1 combination reduced *sost* gene expression by 61% (p=0.006 vs veh,F=3.452, p=0.023). Highly variable *dkk1* expression in the vehicle group obfuscated reduction by each injection group. In addition, we determined the potential regulation of *dkk1* by scl-ab and vice versa because dkk1 and sclerostin share the capacity to bind the first propeller of LRP5/6 or may compensatorily upregulate the other. Neither injection of antibody significantly regulated the transcription of the other antibody's precursor in the IVD. Heat shock protein a1b (*hspa1b*) gene expression in the IVD was not different between groups but scl-Ab trended to reduce *hspa1b* (p=0.069). *Hspa1b* and *serpinA1a* were similarly regulated by each antibody injection (R=0.83, p<0.05) but neither *hspa1b* (F=2.43 and p=0.11), *serpina1a* (F=1.58 and p=0.23), nor *aggrecan* (F=1.70 and p=0.21) expression were changed by any injection compared to vehicle (Fig. 3B). Inflammation-related markers *cxcl9* and *il-1*β were not detected in any IVD.

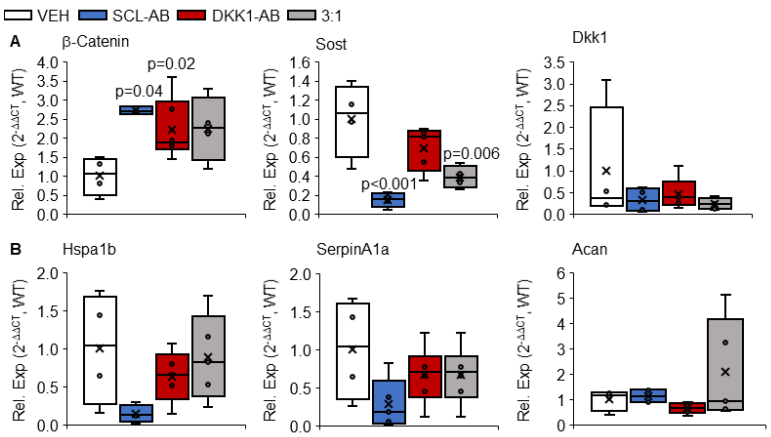

Figure 3. Injection of scl-Ab and/or dkk1-Ab increased pro-Wnt signaling gene expression.

(A) Gene expression related to Wnt signaling in tail IVD: *β-catenin*, *sost*, and *dkk1*. Gene expression of β-catenin in the 3:1 combination injection was trending toward significance (p=0.061) (B) Heat shock protein *hspa1b*, inflammatory marker *serpinA1a*, and ECM marker *aggrecan* expression in the IVD. Scl-ab injection trended to decrease gene expression of *hspa1b* (p=0.069). Injection groups (veh: n=4, scl-Ab: n=5, dkk1-Ab: n=6, and 3:1: n=5) were compared to the vehicle group using a Dunnett's test, with significance noted below $p<0.05$.

Anti-sclerostin-antibody injection increased *β-catenin* protein and reduced mature NP gene expression in the IVD.

Based on the mechanical property improvements by scl-Ab, low variability of upregulation of *β-catenin* by scl-Ab and trending downregulation of *hspa1b*, we further characterized ECM transcription and cell phenotype in the IVD by scl-Ab. Injection of scl-Ab decreased the gene expression of *col1a1* by 57% (p=0.002), *col2a1* by 54% (p=0.02) and *osterix* by 35% (p=0.049) (Fig. 4). Further, scl-ab increased the number of cells expressing β-catenin protein in the nucleus pulposus by 81% (p=0.004) and reduced the number of nucleus pulposus cells that expressed *col2a1* by 46% (p=0.01) (Fig. 5). Similar to *hspa1b,* scl-Ab decreased the gene expression of *hspa1a,* a gene associated with cellular stress,[31] by 95% (p=0.02)

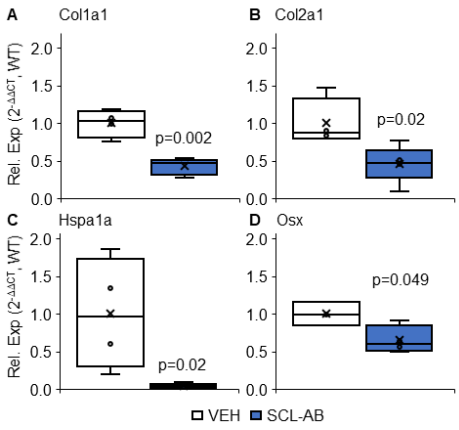

Figure 4. Scl-ab injection reduced ECM, heat shock protein, and osterix gene expression in the IVD. Gene expression of scl-ab injection (n=5) compared to the vehicle-treated tail IVD (n=4) for (A) *cola1a,* (B) *col2a1,* (C) *hspa1a,* and (D) *osx.* Student's t-tests compared groups, with significance noted below p<0.05.

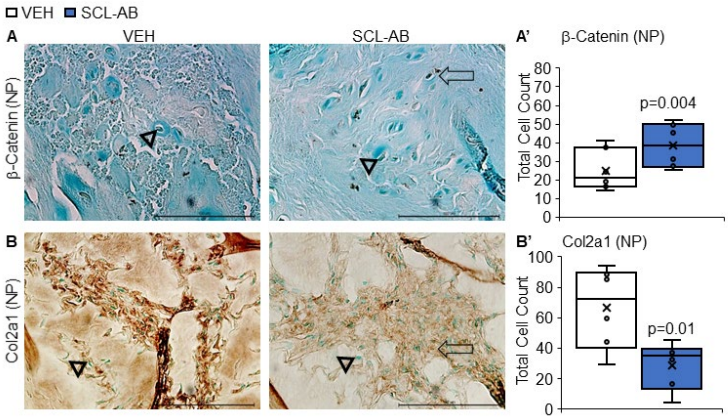

Figure 5. Scl-ab injection promoted β-catenin protein expression in the nucleus pulposus. (A) Images of β-catenin protein expression in the NP of the tail IVD of vehicle (n=7) and anti-sclerostin antibody group (n=6). (A') Quantitative measurements of the fraction of β-catenin protein expressing cells to the total number of cells in the NP. (B) Images of col2a1 protein expression in the NP of the vehicle (n=6) and sclerostin antibody group (n=6). (B') Quantitative measurements of the fraction of col2a1 protein expressing cells to the total number of cells in the

NP. Scale bar: 100 μm. Student's t-tests compared groups, with significance noted below p<0.05.

Systemic deletion of *sost* reduced sclerostin gene and protein expression in the IVD.

Quantitatively, *sost* gene expression was consistently detectable in the WT IVD but *sost* was not detected in any of the *sost* KO IVD (Fig. 6A). Qualitatively, sclerostin protein expression (brown staining, black arrow) appeared in the NP cells of WT IVD (Fig. 6B). By contrast, sclerostin staining in the *sost* KO was minimally expressed in NP cell nuclei and relegated to the cell membrane and extracellular matrix (Fig. 6C). The AF minimally expressed sclerostin (Fig. 6D).

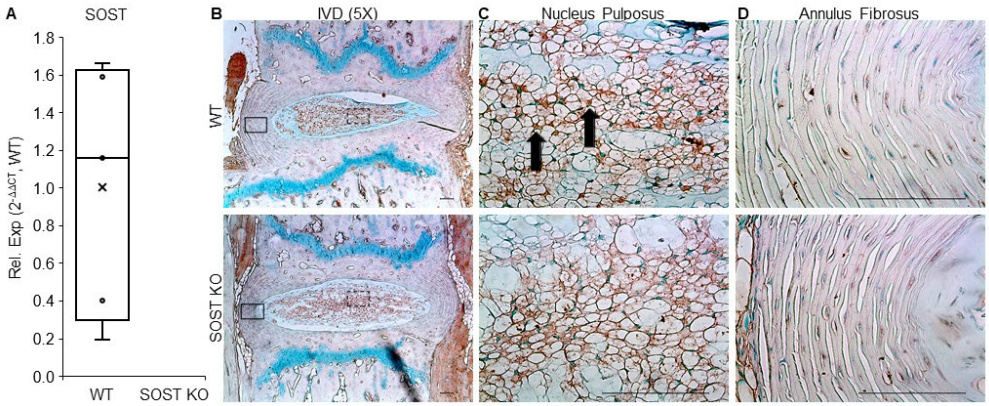

Figure 6. Sost deletion reduced sost gene and protein expression in the IVD. *Sost* gene expression from qPCR and qualitative images of sclerostin staining of the WT and *sost* KO IVD (n = 5) was effectively deleted from the *sost* KO group. (A) qPCR of *sost* from WT IVD (CT: 34.09-34.87, 25-75%). *Sost* gene expression was not detected in sost KO IVD. (B) 40X magnification images of the NP of the WT IVD (top) and *sost* KO IVD (bottom) using Alcian blue counterstain to show sclerostin protein expression in the cells of the IVD. The WT expressed defined dark brown staining (black arrows) while the *sost* KO cells expressed less, more diffuse staining, indicating less sclerostin expression in the *sost* KO. (C) 40X magnification image of the AF. Scale bar: 100μm. Dashed box represents the highlighted NP portion (panel C). Solid box represents the highlighted portion of the AF (panel D).

Deletion of *sost* in the IVD increased IVD height, proteoglycan staining and hydration.

Proteoglycans are hydrophilic proteins and loss of proteoglycans is a common feature of IVD degeneration.[32,33] Compared to WT IVD, deletion of *sost* KO increased lumbar IVD height by 21% (p=0.007) and tail proteoglycan staining by 150% (p=0.02) in the NP (Fig. 7A-C). However, the accumulation of proteoglycan staining, while potentially beneficial for hydration, led to slight disorganization of the band of cells in the NP, statistically insignificantly increasing the histological IVD degeneration score (supplemental figure 2). Next, we determined the hydration of the IVD by MRI, a standard non-invasive clinical imaging technique for determining the morphology and hydration of the IVD (Fig. 6).[34,35] WT IVD had patched distribution of water, while the ring of water that demarcated the cell band from the AF was clearer and brighter in the *sost* KO IVD (Fig. 8). Relative to the WT IVD, *sost* KO increased the estimated water content, i.e., hydration, by 72% (p=0.04) but there was no statistical difference in the total area of the IVD or intensity of the water between groups (Fig. 8, Table 4). These data show that deletion of *sost* imbibed the IVD.

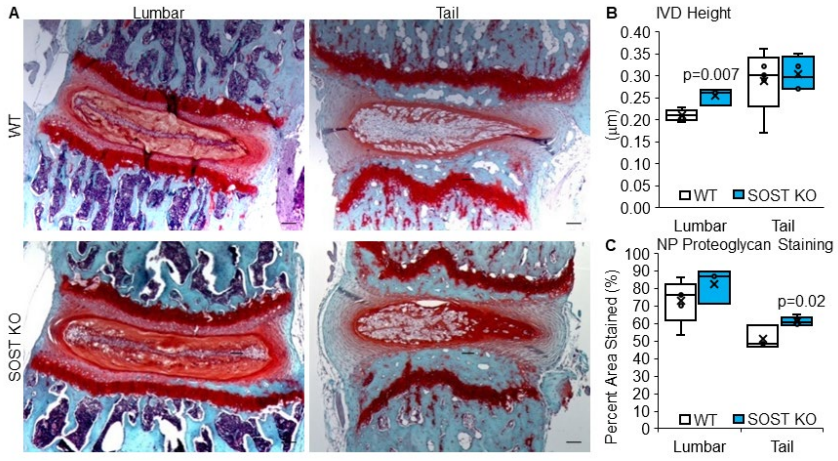

Figure 7. Deletion of *sost* promoted IVD height and proteoglycan staining. (A) 5X

magnification images of Safranin-O and Fast Green counterstain of lumbar and tail IVD (left column, middle column) of the WT group (top row) and *sost* KO group (bottom row, n=5/group). Scale bar: 100 μm. (B) Quantitative measurement of the intensity of proteoglycan staining in the IVD. Red staining indicated proteoglycan. (C) Quantitative measurement of IVD degeneration score for lumbar and tai IVD of the WT and *sost* KO groups. Student's t-tests compared groups, with significance noted below $p<0.05$.

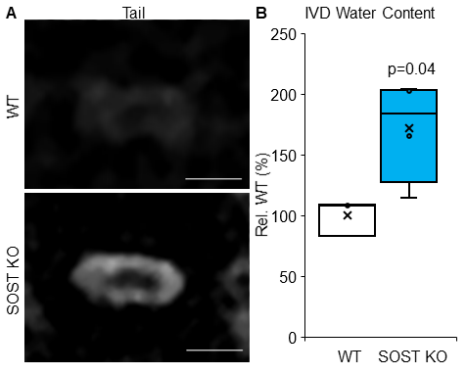

Figure 8. Deletion of *sost* increased IVD hydration. (A) Using a 9.4T MRI, tail motion segments were imaged, highlighting the IVD of the WT (top, n=3) and sost KO (bottom, n=4/group). Scale bar: 1 mm. (B) Relative water content was quantified as the area multiplied by intensity, indicating increased hydration in the KO. Student's t-tests compared groups, with significance noted below $p<0.05$.

Table 3. Area, Intensity, and Water Content Determined by MRI in WT and *sost* KO IVD

Genotype	Area (mm^2)	Intensity	Water Content
WT 1	0.32	956	301.12
WT 2	0.32	1235	395.20
WT 3	0.32	1004	391.56
WT AVG	**0.34 ± 0.04**	**1065 ± 149**	**362.63 ± 52.29**
SOST KO 1	0.65	1145	739.67
SOST KO 2	0.64	1155	733.43
SOST KO 3	0.34	1225	416.50
SOST KO 4	0.40	1501	600.40
SOST KO AVG	**0.51 ± 0.16**	**1257 ± 167**	**622.50 ± 151.61***

Student's t-tests compared groups, with significance noted below p<0.05 (*).

Sost deletion induced compensatory normalization of Wnt signaling by upregulation of Wnt signaling inhibitors.

Canonical Wnt signaling requires translocation of β-catenin to the cell nucleus. Therefore, we determined the nuclear and cytoplasmic fraction of β-catenin protein. *Sost* KO IVD had less active β-catenin protein in the cell nuclei than WT IVD (Fig. 9A), suggesting *less* Wnt signaling. The cytoplasmic fraction was not statistically different between groups (supplemental figure 3). In addition, dkk1 is a target of Wnt/β-catenin signaling so we also determined the gene expression of Wnt inhibitors. Sost KO IVD expressed greater *dkk1* by 10-fold (p=0.04) and *sfrp4* by 4-fold (p<0.001, Fig. 9B). Lack of gene expression difference of co-transcription factor *β-catenin* between WT and sost KO suggests compensation of Wnt signaling following deletion of *sost*.

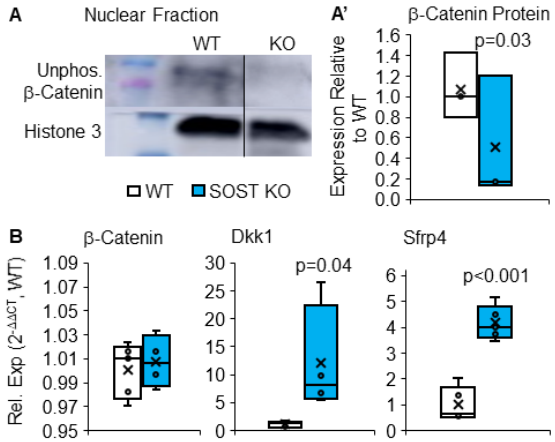

Figure 9. Deletion of sost induced compensation of Wnt signaling by upregulation of wnt signaling inhibitors. (A) Nuclear separation western blotting (composite image from the same blot) showed a decreased amount of active β-catenin in the cell nuclei of the *sost* KO, using Histone 3 as control (n=5/group). (A') Quantitative measurement of β-catenin protein expression from western blot. Unphosphorylated (active) β-catenin at 92 kDa, Histone 3 at 17 kDa, β-actin at 92 kDa. (B) While β-catenin is unchanged, *dkk1* and *sfrp4*, both inhibitors of the pathway, were increased in response to *sost* deletion. Student's t-tests compared groups, with significance noted below $p<0.05$.

Table 4. Genes not significantly regulated by *sost* deletion or expressed in the IVD.

Gene	WT	*Sost* KO	p-value
SerpinA1C+	1 ± 0.18	0.72 ± 0.09	0.06
SerpinA1D	1 ± 0.56	0.52 ± 0.19	0.11
Sostdc1	1 ± 0.35	1.86 ± 0.71	0.11
Keratin8	1 ± 0.83	0.50 ± 0.50	0.26
Wnt 16	1 ± 0.69	1.79 ± 1.46	0.36
Axin 2	1 ± 0.53	1.38 ± 0.75	0.38
SerpinA1A	1 ± 0.37	0.52 ± 0.19	0.80
Cxcl9	Undetermined	Undetermined	N/A
IL1b	Undetermined	Undetermined	N/A

Wnt 3a	Undetermined	Undetermined	N/A

Student's t-tests compared groups, with significance noted below 0.05. N/A: Not applicable

Compensation of Wnt signaling from *sost* deletion triggered extracellular matrix degradation and the expression of a mature NP cell phenotype in the IVD.

Sost KO regulated gene and protein expression of extracellular matrix metabolism towards anti-anabolism, catabolism and IVD cell phenotypes toward chondrogenesis. Specifically, deletion of *sost* downregulated gene expression of *aggrecan* 52% (p=0.03) (Fig. 10A). Common markers of notochordal cells and mature NP cells were determined, respectively. *Sost* KO IVDs expressed less transcription of notochordal marker *foxA2*[36] by 77% (p=0.01), less transcription of early NP marker *col2a1* by 67% (p=0.05), and fewer cells in the NP expressed *col2a1* (Fig. 11A, A'). By contrast, accrual of mature NP can be marked by increased chondrogenic marker[37] and osteoblast transcription factor Sp7 (Osx). Compared to WT IVD, *sost* KO IVD expressed increased osterix gene expression by 4.4-fold (p=0.03) and protein expression (Fig. 10B, 11B, B'). Sost deletion similarly altered gene expression in lumbar IVD from rna-seq with upregulation of ECM degradation, downregulation of notochordal marker *gdf5*[38], downregulation of early mature NP markers (*ColX*[39]) and upregulation of mature NP cell marker *bglap* (Supplemental Figure 4). Gene expression that was not statistically different between WT and *sost* KO IVD included *serpinA1a-c* (*serpinA1c+*, p=0.06), *serpinA1d*, *sostdc1*, *keratin8*, *wnt16*, *axin2*, *serpinA1a*, *cxcl9*, *il-1β* and *wnt3a* (Table 3).

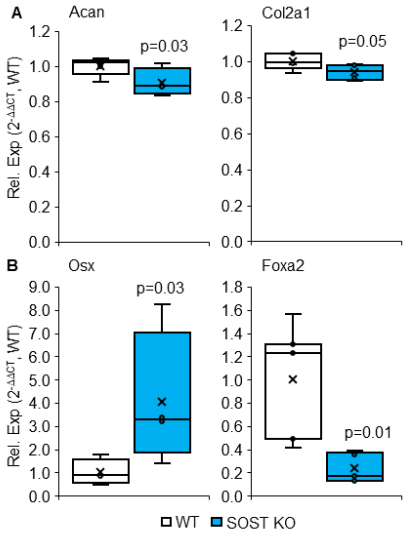

Figure 10. Global deletion of *sost* induced the gene expression of a mature cell type in the IVD. Gene expression of (A) ECM and (B) transcription factors of cell type markers in WT and sost KO IVD (n=5, group). Student's t-tests compared groups, with significance noted below $p<0.05$.

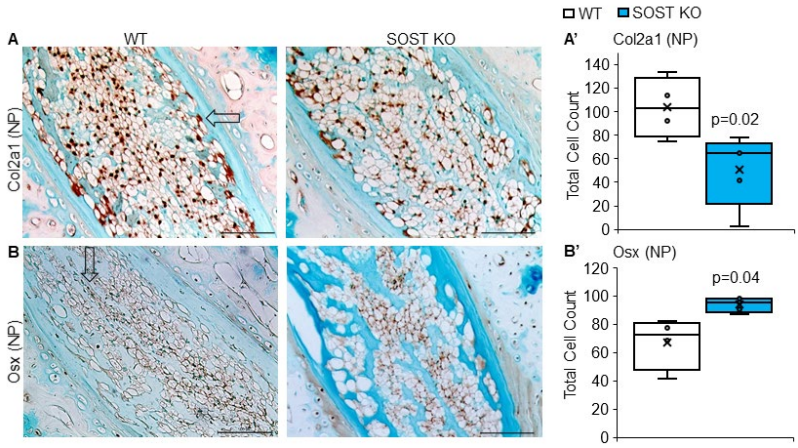

Figure 11. Global deletion of *sost* induced the protein expression of a mature NP cell phenotype. (A) Collagen 2 staining and (B) osterix staining of the NP of the WT and *sost* KO (n=5/group). Quantitative measurement of the fraction of the number of positively (brown) stained (arrow) (A') collagen 2 expressing cells and (B') osterix expressing cells. Student's t-tests compared groups, with significance noted below $p<0.05$.

Using whole transcriptomic analysis, sost deletion downregulated pathways related to protein folding and upregulated pathways related to immune response in the IVD.

In an overall sense, based on the PCA plot (Fig. 12A), *sost* KO IVDs are not transcriptomically distinct to WT IVDs. Nevertheless, 35% of the top 20 downregulated pathways were related to cellular response to external stimuli (e.g., protein folding, FDR<0.05), 15% to metabolism, 15% to extracellular matrix organization, 10% to gene expression, and 5% to developmental biology, signaling transduction, metabolism of proteins, transportation of small molecules, and other pathways (Fig. 12B). Whereas, of the top 20 upregulated pathways, 85% were related to immune pathways (FDR<0.05), and 5% each to cell cycle (FDR<0.05), signaling transduction (FDR<0.05), and hemostasis (FDR<0.05). Specifically, the heat map for the top downregulated pathway was 'protein folding', which included heat shock proteins, and for the top upregulated pathway was immune response (Fig. 12C). More specifically, the volcano plot highlights in red the genes that were most significantly differentially regulated (Fig. 12D). A list of the top 20 differentially downregulated and top 20 upregulated were included (Table 5, 6). Lastly, GSEA analysis for the *sost* KO IVDs corroborated that Wnt signaling was reduced based on the normalized enrichment score (-1.53, FDR<0.01, Table 7 and 8, supplemental figure 5).

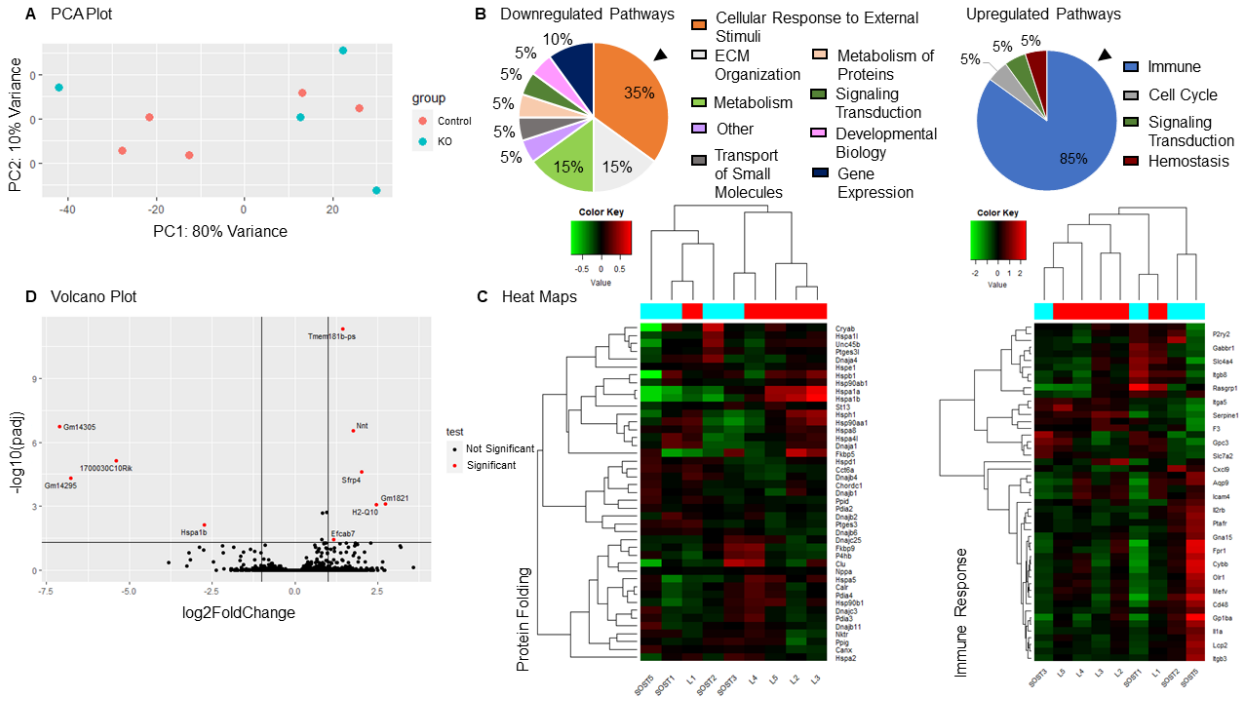

Figure 12. RNA sequencing of sost KO and WT IVD. (A) PCA plot of *sost* KO (n=4) and WT (n=5) IVDs demonstrating an overlap between the groups. (B) Top 20 down-regulated and top 20 up-regulated pathways following *sost* deletion. (C) Corresponding heat maps for protein folding associated with the top downregulated pathway (arrowhead in B) and immune response associated with the top upregulated pathway (arrowhead in B). (D) Volcano plot of all differentially regulated genes, with labels of most significantly regulated genes (FDR<0.05).

Table 5. Top 20 genes upregulated by *sost* KO.

Gene	Fold Change	p-value	FDR
Ntn	3.34	<0.001	<0.001
Tmem181b-ps	2.66	<0.001	<0.001
Sfrp4	3.97	<0.001	<0.001
Gm1821	6.58	<0.001	0.002
H2-Q10	5.36	<0.001	0.007
Wdfy1	1.90	<0.001	0.091
Mepe	3.66	<0.001	0.149
Clec10a	3.49	<0.001	0.233

Sp6	2.85	<0.001	0.268
Cd1d1	2.53	<0.001	0.340
Fasn	2.91	<0.001	0.340
Tnfrsf19	1.79	<0.001	0.359
Scd1	3.43	<0.001	0.364
Dgat2	2.27	<0.001	0.364
Serping1	1.93	<0.001	0.371
Agppat2	1.94	<0.001	0.421
Cxcl9	3.35	0.001	0.512
Cebpa	1.95	0.001	0.513
Efcab7	2.21	0.001	0.513
Myh7	33.95	0.001	0.513

Table 6. Top 20 genes downregulated by *sost* KO.

Gene	Fold Change	p-value	FDR
Gm14305	-109.99	<0.001	<0.001
Gm14295	-153.71	<0.001	<0.001
1700030C10Rik	-37.64	<0.001	<0.001
Hspa1b	-6.72	<0.001	0.051
Hist1h1b	-7.38	<0.001	0.254
Hsph1	-2.34	<0.001	0.286
Rec8	-8.73	<0.001	0.286
Eps8l1	-3.69	<0.001	0.286
Rn45s	-4.57	<0.001	0.286
Hspa1a	-4.52	0.001	0.513
Aldh3a1	-2.97	0.001	0.513
Serpine1	-3.13	0.001	0.513
Slc15a2	-9.53	0.002	0.565
Nfatc2	-1.93	0.002	0.656
Erdr1	-3.21	0.002	0.656
Foxa2	-2.34	0.003	0.656
Gm7120	-2.08	0.003	0.776
Egr1	-1.75	0.003	0.788
Hsp90aa1	-1.96	0.005	1.000
Gdf5	-2.98	0.006	1.000

Table 7. Top 20 down-regulated pathways by *sost* deletion

Name	Normalized Enrichment Score	Nominal p-value	FDR
INTERFERON α-RESPONSE	-1.57	<0.001	0.007
BILE ACID METABOLISM	-1.56	<0.001	0.006
NOTCH SIGNALING	-1.56	0.010	0.006
WNT β-CATENIN SIGNALING	-1.53	0.011	0.008
PEROXISOME	-1.52	0.001	0.009
ALLOGRAFT REJECTION	-1.51	0.001	0.010
INTERFERON γ-RESPONSE	-1.47	0.000	0.016
UV RESPONSE DN	-1.39	0.006	0.036
XENOBIOTIC METABOLISM	-1.36	0.006	0.047
FATTY ACID METABOLISM	-1.32	0.013	0.072
KRAS SIGNALING UP	-1.30	0.006	0.082
ADIPOGENESIS	-1.29	0.004	0.089
COAGULATION	-1.26	0.059	0.118
IL6 JAK STAT3 SIGNALING	-1.23	0.112	0.161
INFLAMMATORY RESPONSE	-1.16	0.133	0.317
ANGIOGENESIS	-1.15	0.263	0.311
HEDGEHOG SIGNALING	-1.11	0.326	0.441
OXIDATIVE PHOSPHORYLATION	-1.09	0.226	0.479
APICAL JUNCTION	-1.09	0.243	0.478
COMPLEMENT	-1.09	0.262	0.462

Sost KO and scl-ab increased vertebral bone structure

Osteocytes and osteoblasts are the predominate sclerostin-expressing cells.[13,40] Here, WT tail vertebra expressed sclerostin staining in both osteocytes and osteoblasts while global deletion of *sost* blunted its expression in the vertebra (Supplemental Figure 6) and, consequently, increased trabecular and cortical bone structure (Table 8). Scl-ab may have induced a compensatory upregulation of sclerostin protein (Supplemental Figure 7). Separately, scl-Ab increased the number of osteocytes expressing substance P because of the need for innervation during bone formation.[41]

Table 8. *Sost* KO vertebral bone structural properties.

Bone Parameter	Tail		Lumbar	
	WT	*sost* KO	WT	*sost* KO
Tb.BV/TV (%)	49.4 ± 3.1	53.5 ± 4.6	**25.3% ± 4.8**	**45.7 ± 5.1***
Tb.N (1/mm)	5.52 ± 0.30	5.84 ± 0.14	6.11 ± 0.50	6.45 ± 0.76
Tb.Th (mm)	0.09 ± 0.01	0.09 ± 0.01	0.07 ± 0.01	0.07 ± 0.01

Discussion

FDA-approved anti-sclerostin antibody (scl-Ab) augmented the structure and strength of the IVD. We hypothesized that increasing Wnt signaling by suppression of Wnt competitors by pharmacological or genetic approaches would augment the structure of the IVD. Sclerostin and dkk1 are known inhibitors of the canonical Wnt signaling pathway and work in a similar fashion.[42] Scl-Ab, dkk1-Ab, and the 3:1 combinatorial injection of sclerostin and dkk1 increased lumbar IVD height via strong upregulation of Wnt/□-catenin signaling but injection of a 1:1 ratio of sclerostin to dkk1 antibody or a 1:3 ratio were not as beneficial. By contrast, only scl-ab injection improved the mechanical properties of the IVD. Prolonged suppression of sclerostin by global deletion of *sost* increased IVD height, water content and proteoglycan staining but induced a significant normalization of Wnt signaling. Overall, these data show that systemic administration of scl-Ab promotes major features of the IVD that are lost with IVD degeneration.

Sclerosteosis patients with a sost gene mutation are associated with greater bone mass and stature.[43] Although mice with injection of scl-Ab,[44] conditional deletion of sost in bone cells or global KO of sost all have greater bone mass, vertebral bone length does not change.[45] Therefore,

neutralization of sost/sclerostin may extend IVD height by direct stimulation of Wnt signaling and/or adaptation to greater bone mass.

IVD cells express Wnt signaling inhibitors *sost*/sclerostin and dkk1[11] but their role in the IVD was undetermined. Nucleus pulposus-specific upregulation and downregulation of Wnt signaling co-transcription factor β-catenin is anabolic and catabolic to the ECM/stiffness of the IVD, respectively.[12] Here, injections of scl-Ab, dkk1-Ab and in combination increased IVD height and β-catenin gene expression. We also administered combinatorial injections of scl-Ab and dkk1-Ab (3:1, 1:1 and 1:3), where 3:1 injection outperformed 1:1 and 1:3 injections in increasing IVD height. Therefore, we excluded 1:1 and 1:3 injections from further examination. The 3:1 injection most closely approximated the WT gene expression of sost relative to dkk1, which could have most effectively neutralized sclerostin and dkk1 to upregulate Wnt/β-catenin signaling in the IVD.

Our data and others have noted that sclerostin and dkk1 share a mutual compensatory regulation of the Wnt/β-catenin signaling pathway,[11,12,20] which may impact IVD cell differentiation. We found that global sost deletion induced a strong upregulation of Wnt signaling inhibitors that consequently normalized β-catenin protein in IVD cell nuclei and Wnt signaling. Normalization of Wnt signaling may have attenuated the initial benefits of activation and could explain the subdued difference between *sost* KO and WT IVD. Similarly, we noted compensation of sclerostin in osteocytes of sclerostin-antibody treated mice. Next, we previously found that similar to ECM anabolism,[12] regulation of Wnt signaling in the IVD was associated with differential regulation of cell type expression (notochordal cell, e.g., brachyury, vs mature NP cell, e.g., osterix).

Conditional stabilization of β-catenin in nucleus pulposus cells using a Shh-CreERT2 driver promotes brachyury and reduces osterix, whereas deletion of β-catenin using the Shh-CreERT2 driver reduces brachyury and promotes osterix. Similarly, here, stimulation of Wnt signaling by scl-ab promoted β-catenin and reduced osterix but Wnt signaling compensation following sost deletion reduced notochordal markers (*krt19*, *foxa2*[46], and *gdf5*[38]) and increased mature NP cell markers (osterix[21] and bglap). Therefore, persistent suppression of sclerostin may need to be avoided to limit potential compensatory cell differentiation in healthy IVD and it is unclear if this compensation would occur in degenerated IVD.

IVD degeneration is characterized by IVD height loss from proteoglycan breakdown and dehydration,[47,48] which is necessary for the IVD to withstand spinal mechanical forces and function properly. While many of the combinations tested here similarly upregulated β-catenin gene expression and IVD height, scl-Ab injection alone most functionally strengthened the IVD. In corroboration, deletion of *sost* increased the proteoglycan staining in the nucleus pulposus and increased water content, as measured by MRI. These data suggest that regulation of sclerostin may have additional downstream effects from canonical Wnt signaling that impact the material mechanical properties of the IVD.

Although sclerostin and dkk1 are both inhibitors of canonical Wnt signaling, sclerostin and dkk1 can inhibit different Wnt ligands[42] and impose distinct regulation of targets. Our data suggest that they may distinctly regulate heat shock protein (Hsp) expression and other genes related to protein folding. Crosstalk between Hsps and Wnt signaling has been previously proposed to mediate axial

patterning and cell proliferation, where long-term induction of Hsps reduces Wnt targets brachyury, tcf and Wnt3.[49] In the IVD, hsps are responsive to environmental stresses[31] and are differentially regulated by mechanical strain.[47] For instance, loss of mechanical signals by cellular disanchoring reduces *hsp* gene expression and compressive mechanical strains upregulate *hsp* gene expression in nucleus pulposus cells.[50] *Hspa1a* and *hspa1b* are both expressed in the IVD[51] and, although scl-Ab and dkk1-Ab induced similar upregulation of β-catenin, only scl-Ab downregulated *hsps*. Similarly, *sost* deletion reduced *hsp*s even though Wnt signaling was normalized in these IVDs. These data suggest that neutralization of sclerostin reduces hsps, rather than by activation of Wnt signaling itself.

We would like to address some of the limitations of the study. First, scl-Ab is prescribed to postmenopausal women and while we injected female mice, our KO mice were males. Nevertheless, we expect similar effects of *sost* deletion in female IVD.[8,20] Future experiments will include determining the effect of anti-sclerostin injections to counter challenges to the disc, e.g., aging and injury, and the ability of systemic injection of anti-sclerostin to reach the IVD. Secondly, qPCR was performed on entire IVDs and the effect of *sost* KO could not be differentiated by gene expression, but key outcomes were further discerned in a localized manner using immunohistochemistry. While we did not note any histological protein changes of β-catenin nor sclerostin in the annulus fibrosus by regulation of sost/sclerostin, a more localized approach may discern these potential changes. Further, proteoglycan content estimation by histology will require corroboration. Thirdly, silencing Wnt signaling in IVD cells induces ECM degradation,[20,52] but also promotes anti-inflammation.[53] By contrast, activating Wnt signaling in murine IVD leads to elevated ECM production,[54] but also promotes pro-inflammatory signals.[53] Based on ECM

metabolism, our data suggest that Wnt signaling was increased by anti-Wnt signaling inhibitor injection and sost deletion (at least initially), but *sost* deletion also induced upregulation of immune pathways. Injection of scl-ab did not upregulate immune-related genes, therefore, the pulsatile upregulation of Wnt signaling by scl-Ab as occurs clinically may preclude the consequences of an inflammatory response. Despite these limitations, we show that upregulation of Wnt signaling by persistent and long-term absence of *sost* hydrates the IVD and promotes ECM expression in lumbar IVD, but compensation of Wnt signaling may induce mild mature cell differentiation.

In conclusion and in addition to the well-recognized attributes to bone structure, suppression of *sost*/sclerostin or dkk1 augmented IVD structure. Combinatorial injection of scl-Ab and dkk1-Ab similarly increased IVD height as each alone, when the ratio of the administration reflected in vivo ratios, but scl-Ab alone most strengthened the IVD. Persistent genetic deletion of *sost* increased proteoglycan staining and IVD hydration but also induced a compensatory upregulation of Wnt signaling inhibitors that consequently normalized Wnt signaling. Together, these data show that the musculoskeletal benefits of scl-ab romosozumab (Evenity), which is commercially available, may extend beyond bone to improve key features of the IVD and could potentially be used as a therapeutic for IVD degeneration.

Acknowledgments

Funding: Biomedical Research Grant (EC), Biomechanics and Biomaterials Research Center grant (NH), Start-up (NH), ORS Spine Section Travel Fellowship (NB). We would like to thank the Indiana Center for Musculoskeletal Health (ICMH) for their support. In addition, we would like to thank Washington University in St. Louis for access to the Structure and Strength Core. Data

and materials availability: All data associated with this study are present in the paper or Supplementary Materials.

Figure Legends

Figure 1. Qualitative and quantitative lumbar IVD structural measurements. (A) 5X magnification images of Safranin-O and Fast Green counter stained histological sections of the lumbar IVD for vehicle (VEH, n = 5 mice), 25 mg/kg sclerostin-antibody injection (SCL-AB, n=5), 25 mg/kg injection of dkk1-antibody (DKK1-AB, n=5) (top row, left to right), combination injection of 18.75 mg/kg sclerostin-antibody and 6.25 mg/kg dkk1-antibody (3:1, n=5), combination of 12.5 mg/kg each of sclerostin- and dkk1-antibody (1:1, n=7), and a combination injection of 6.25 mg/kg of sclerostin-antibody and 18.75 mg/kg of dkk1-antibody (1:3, n=6) (bottom row, left to right). (B) Quantitative measurement of lumbar IVD height of all 6 groups. (C) Quantitative measurement of proteoglycan intensity staining in percentage of the lumbar IVD. Red staining indicating proteoglycan content. Scale bar is 100 μm. Injection groups were compared to the vehicle group using a Dunnett's test, with significance noted below $p<0.05$.

Figure 2. Injection of scl-Ab improved IVD mechanical properties. C57Bl6 mice were injected with vehicle (VEH, n = 7 mice), 25 mg/kg sclerostin-antibody injection (SCL-AB, n=6), 25 mg/kg injection of dkk1-antibody (DKK1-AB, n=7), combination injection of 18.75 mg/kg sclerostin-antibody and 6.25 mg/kg dkk1-antibody (3:1, n=6), combination of 12.5 mg/kg each of sclerostin- and dkk1-antibody (1:1, n=7), or a combination injection of 6.25 mg/kg of sclerostin-antibody and 18.75 mg/kg of dkk1-antibody (1:3, n=7). (A) Loading

stiffness, (B) unloading stiffness, (C) ultimate force, (D) energy dissipation, (E) displacement and (F) loss tangent of the IVD. Injection groups were compared to the vehicle group using a Dunnett's test, with significance noted below $p<0.05$.

Figure 3. Injection of scl-Ab and/or dkk1-Ab increased pro-Wnt signaling gene expression. (A) Gene expression related to Wnt signaling in tail IVD: *β-catenin*, *sost*, and *dkk1*. Gene expression of β-catenin in the 3:1 combination injection was trending toward significance ($p=0.061$) (B) Heat shock protein *hspa1b*, inflammatory marker *serpina1a*, and ECM marker *aggrecan*. Scl-ab injection decreased gene expression of *hspa1b* trending toward significance ($p=0.069$). Injection groups (VEH n=4, SCL-AB n=5, DKK1-AB n=6, and 3:1 n=5) were compared to the vehicle group using a Dunnett's test, with significance noted below $p<0.05$.

Figure 4. Scl-ab injection reduced ECM, heat shock protein, and osterix gene expression in the IVD. Gene expression of scl-ab injection (n=5) compared to the vehicle-treated tail IVD (n=4) for (A) *cola1a,* (B) *col2a1,* (C) *hspa1a,* and (D) *osx.* Student's t-tests compared groups, with significance noted below $p<0.05$.

Figure 5. Scl-ab injection promoted β-catenin protein expression in the IVD. (A) Images of β-catenin protein expression in the NP of the tail IVD of vehicle (n=7) and sclerostin antibody group (n=6). (A') Quantitative measurements of the fraction of β-catenin protein expressing cells to the total number of cells in the NP. (B) Images of col2a1 protein expression in the NP of the vehicle (n=6) and sclerostin antibody group

(n=6). (B') Quantitative measurements of the fraction of col2a1 protein expressing cells to the total number of cells in the NP. Scale bar: 100 μm. Student's t-tests compared groups, with significance noted below $p<0.05$.

Figure 6. Sost deletion reduced sost gene and protein expression in the IVD.

Sost gene expression from qPCR and qualitative images of sclerostin staining of the WT and *sost* KO IVD (n = 5) is effectively deleted from the *sost* KO group. (A) qPCR of *sost* with *sost* KO being normalized and compared to the WT (CT: 34.09-34.87, 25-75%). *Sost* gene expression was not detected in sost KO IVD. (B) 40X magnification images of the NP of the WT IVD (top) and *sost* KO IVD (bottom) using Alcian blue counterstain to show sclerostin protein expression in the cells of the IVD. The WT expressed defined dark brown staining (black arrows) while the *sost* KO cells expressed less, more diffuse staining, indicating less sclerostin expression in the *sost* KO. (C) 40X magnification image of the AF. Scale bar: 100μm. Dashed box represents the highlighted NP portion (panel C). Solid box represents the highlighted portion of the AF (panel D).

Figure 7. Deletion of *sost* promoted IVD height proteoglycan staining. (A) 5X magnification images of Safranin-O and Fast Green counterstain of lumbar and tail IVD (left column, middle column) of the WT group (top row) and *sost* KO group (bottom row, n=5/group). Scale bar: 100 μm. (B) Quantitative measurement of the intensity of proteoglycan staining in the IVD. Red staining indicating proteoglycan content. (C) Quantitative measurement of IVD degeneration score for lumbar and tai IVD of the WT and *sost* KO groups. Student's t-tests compared groups, with significance noted below $p<0.05$.

Figure 8. Deletion of *sost* increased IVD hydration. (A) Using 9.4T MRI, tail motion segments were imaged highlighting the IVD of the WT (top, n=3) and sost KO (bottom, n=4/group). Scale bar is 1 mm. (B) Relative water content quantitatively measured, using area multiplied by intensity, indicating increased hydration in the KO. Student's t-tests compared groups, with significance noted below $p<0.05$.

Figure 9. Deletion of sost induced compensation of Wnt signaling by upregulation of Wnt inhibitors. (A) Nuclear separation western blot (composite image from the same blot) shows decreased amount of active β-catenin in the cell nuclei of the *sost* KO, using Histone 3 as control (n=5/group). (A') Quantitative measurement of β-catenin protein expression from western blot. Unphosphorylated (active) β-catenin at 92 kDa, Histone 3 at 17 kDa, β-actin at 92 kDa. (B) While β-catenin is unchanged, *dkk1* and *sfrp4*, both inhibitors of the pathway, are both increased in response to the *sost* KO. Student's t-tests compared groups, with significance noted below $p<0.05$.

Figure 10. Global deletion of *sost* induced the gene expression of a mature cell type in the IVD. Gene expression of (A) ECM and (B) transcription factor cell type markers in WT and sost KO IVD (n=5, group). Student's t-tests compared groups, with significance noted below $p<0.05$.

Figure 11. Global deletion of *sost* induced the protein expression of a mature NP cell phenotype. (A) Collagen 2 staining and (B) osterix staining of the NP of the WT and *sost* KO (n=5/group). Quantitative measurement of the fraction of the number of positively

(brown) stained (black arrow) (A') collagen 2 expressing cells and (B') osterix expressing cells. Student's t-tests compared groups, with significance noted below $p<0.05$.

Figure 12. RNA sequencing of sost KO and WT IVD. (A) PCA plot of *sost* KO (n=4) and WT (n=5) IVDs demonstrating an overlap between the groups. (B) Top 20 down-regulated and top 20 up-regulated pathways following *sost* deletion. (C) Corresponding heat maps for protein folding associated with the top downregulated pathway (arrowhead in B) and immune response associated with the top upregulated pathway (arrowhead in B). (D) Volcano plot of all differentially regulated genes, with labels of most significantly regulated genes (FDR<0.05).

References

1. Basso M, Cavagnaro L, Zanirato A, et al. What is the clinical evidence on regenerative medicine in intervertebral disc degeneration? *Musculoskeletal Surgery*. Published online 2017. doi:10.1007/s12306-017-0462-3

2. Loibl M, Wuertz-Kozak K, Vadala G, Lang S, Fairbank J, Urban JP. Controversies in regenerative medicine: Should intervertebral disc degeneration be treated with mesenchymal stem cells? *JOR SPINE*. Published online 2019. doi:10.1002/jsp2.1043

3. Papavassiliou AG, Pneumaticos SG, Evangelopoulos DS. Biologic treatment of mild and moderate intervertebral disc degeneration. *Molecular Medicine*. Published online 2014. doi:10.2119/molmed.2014.00145

4. Dowdell J, Erwin M, Choma T, Vaccaro A, Iatridis J, Cho SK. Intervertebral disk degeneration and repair. *Clinical Neurosurgery*. Published online 2017. doi:10.1093/neuros/nyw078

5. Livshits G, Ermakov S, Popham M, et al. Evidence that bone mineral density plays a role in degenerative disc disease: The UK twin spine study. *Annals of the Rheumatic Diseases*. Published online 2010. doi:10.1136/ard.2010.131441

6. Cosman F, Crittenden DB, Adachi JD, et al. Cosman F, Crittenden DB, Adachi JD, Binkley N, Czerwinski E, Ferrari S, et al. Romosozumab Treatment in Postmenopausal Women with Osteoporosis. N Engl J Med. 2016; *New England Journal of Medicine*. Published online 2016. doi:10.1056/NEJMoa1607948

7. FDA approves new treatment for osteoporosis in postmenopausal women at high risk of fracture. *Case Medical Research*. Published online 2019. doi:10.31525/fda2-ucm635653.htm

8. Li X, Ominsky MS, Niu QT, et al. Targeted deletion of the sclerostin gene in mice results in increased bone formation and bone strength. *Journal of Bone and Mineral Research*. Published online 2008. doi:10.1359/jbmr.080216

9. Holguin N, Brodt MD, Silva MJ. Activation of Wnt Signaling by Mechanical Loading Is Impaired in the Bone of Old Mice. *Journal of Bone and Mineral Research*. Published online 2016. doi:10.1002/jbmr.2900

10. van Bezooijen RL, Roelen BAJ, Visser A, et al. Sclerostin Is an Osteocyte-expressed Negative Regulator of Bone Formation, but Not a Classical BMP Antagonist. *Journal of Experimental Medicine*. Published online 2004. doi:10.1084/jem.20031454

11. Witcher PC, Miner SE, Horan DJ, et al. Sclerostin neutralization unleashes the osteoanabolic effects of Dkk1 inhibition. *JCI insight*. Published online 2018. doi:10.1172/jci.insight.98673

12. Holguin N, Silva MJ. In-Vivo Nucleus Pulposus-Specific Regulation of Adult Murine Intervertebral Disc Degeneration via Wnt/Beta-Catenin Signaling. *Scientific Reports*. Published online 2018. doi:10.1038/s41598-018-29352-3

13. Holdsworth G, Roberts SJ, Ke HZ. Novel actions of sclerostin on bone. *Journal of Molecular Endocrinology*. Published online 2019. doi:10.1530/JME-18-0176

14. de Boer J, Siddappa R, Gaspar C, van Apeldoorn A, Fodde R, van Blitterswijk C. Wnt signaling inhibits osteogenic differentiation of human mesenchymal stem cells. *Bone*. Published online 2004. doi:10.1016/j.bone.2004.01.016

15. Zhu M, Tang D, Wu Q, et al. Activation of β-catenin signaling in articular chondrocytes leads to osteoarthritis-like phenotype in adult β-catenin conditional activation mice. *Journal of Bone and Mineral Research*. Published online 2009. doi:10.1359/jbmr.080901

16. Bourhis E, Tam C, Franke Y, et al. Reconstitution of a Frizzled8·Wnt3a·LRP6 signaling complex reveals multiple Wnt and Dkk1 binding sites on LRP6. *Journal of Biological Chemistry*. Published online 2010. doi:10.1074/jbc.M109.092130

17. van Dinther M, Zhang J, Weidauer SE, et al. Anti-Sclerostin Antibody Inhibits Internalization of Sclerostin and Sclerostin-Mediated Antagonism of Wnt/LRP6 Signaling. *PLoS ONE*. Published online 2013. doi:10.1371/journal.pone.0062295

18. Ettenberg SA, Charlat O, Daley MP, et al. Inhibition of tumorigenesis driven by different Wnt proteins requires blockade of distinct ligand-binding regions by LRP6 antibodies. *Proceedings of the National Academy of Sciences of the United States of America*. Published online 2010. doi:10.1073/pnas.1007428107

19. Niida A, Hiroko T, Kasai M, et al. DKK1, a negative regulator of Wnt signaling, is a target of the beta-catenin/TCF pathway. *Oncogene*. 2004;23(52):8520-8526. doi:10.1038/sj.onc.1207892

20. Kondo N, Yuasa T, Shimono K, et al. Intervertebral disc development is regulated by wnt/β-catenin signaling. *Spine*. Published online 2011. doi:10.1097/BRS.0b013e3181f52cb5

21. Silva MJ, Holguin N. Aging aggravates intervertebral disc degeneration by regulating transcription factors toward chondrogenesis. *FASEB Journal*. doi:doi.org/10.1096/fj.201902109R

22. Holguin N, Aguilar R, Harland RA, Bomar BA, Silva MJ. The aging mouse partially models the aging human spine: Lumbar and coccygeal disc height, composition, mechanical properties, and Wnt signaling in young and old mice. *Journal of Applied Physiology*. Published online 2014. doi:10.1152/japplphysiol.01322.2013

23. Smolders LA, Meij BP, Riemers FM, et al. Canonical Wnt signaling in the notochordal cell is upregulated in early intervertebral disk degeneration. *Journal of Orthopaedic Research*. Published online 2012. doi:10.1002/jor.22000

24. Cappello R, Bird JLE, Pfeiffer D, Bayliss MT, Dudhia J. Notochordal cell produce and assemble extracellular matrix in a distinct manner, which may be responsible for the maintenance of healthy nucleus pulposus. *Spine*. Published online 2006. doi:10.1097/01.brs.0000209302.00820.fd

25. Li X, Ominsky MS, Warmington KS, et al. Sclerostin antibody treatment increases bone formation, bone mass, and bone strength in a rat model of postmenopausal osteoporosis. *Journal of Bone and Mineral Research*. Published online 2009. doi:10.1359/jbmr.081206

26. Diarra D, Stolina M, Polzer K, et al. Dickkopf-1 is a master regulator of joint remodeling. *Nature Medicine*. Published online 2007. doi:10.1038/nm1538

27. Tam V, Chan WCW, Leung VYL, et al. Histological and reference system for the analysis of mouse intervertebral disc. *Journal of Orthopaedic Research*. Published online 2018. doi:10.1002/jor.23637

28. Liu JW, Abraham AC, Tang SY. The high-throughput phenotyping of the viscoelastic behavior of whole mouse intervertebral discs using a novel method of dynamic mechanical testing. *Journal of Biomechanics*. 2015;48(10). doi:10.1016/j.jbiomech.2015.04.040

29. Holguin N, Brodt MD, Sanchez ME, Silva MJ. Aging diminishes lamellar and woven bone formation induced by tibial compression in adult C57BL/6. *Bone*. Published online 2014. doi:10.1016/j.bone.2014.05.006

30. Clinkenbeard EL, Farrow EG, Summers LJ, et al. Neonatal Iron deficiency causes abnormal phosphate metabolism by elevating FGF23 in normal and ADHR Mice. *Journal of Bone and Mineral Research*. Published online 2014. doi:10.1002/jbmr.2049

31. Chooi WH, Chan SCW, Gantenbein B, Chan BP. Loading-induced heat-shock response in bovine intervertebral disc organ culture. *PLoS ONE*. Published online 2016. doi:10.1371/journal.pone.0161615

Kiani C, Chen L, Wu YJ, Yee AJ, Yang BB. Structure and function of aggrecan. *Cell Research*. Published online 2002. doi:10.1038/sj.cr.7290106

Wei Q, Zhang X, Zhou C, Ren Q, Zhang Y. Roles of large aggregating proteoglycans in human intervertebral disc degeneration. *Connective Tissue Research*. Published online 2019. doi:10.1080/03008207.2018.1499731

34. Marinelli NL, Haughton VM, Muñoz A, Anderson PA. T 2 relaxation times of intervertebral disc tissue correlated with water content and proteoglycan content. *Spine*. Published online 2009. doi:10.1097/BRS.0b013e318195dd44

Grunert P, Hudson KD, Macielak MR, et al. Assessment of intervertebral disc degeneration based on quantitative magnetic resonance imaging analysis: An in vivo study. *Spine*. Published online 2014. doi:10.1097/BRS.0000000000000194

Zhou X, Ma C, Hu B, et al. FoxA2 regulates the type II collagen–induced nucleus pulposus–like differentiation of adipose-derived stem cells by activation of the Shh signaling pathway. *FASEB Journal*. Published online 2018. doi:10.1096/fj.201800373R

37. Minogue BM, Richardson SM, Zeef LAH, Freemont AJ, Hoyland JA. Transcriptional profiling of bovine intervertebral disc cells: Implications for identification of normal and degenerate human intervertebral disc cell phenotypes. *Arthritis Research and Therapy*. Published online 2010. doi:10.1186/ar2929

38. Hodgkinson T, Shen B, Diwan A, Hoyland JA, Richardson SM. Therapeutic potential of growth differentiation factors in the treatment of degenerative disc diseases. *JOR SPINE*. Published online 2019. doi:10.1002/jsp2.1045

39. Aigner T, Greskötter KR, Fairbank JCT, von der Mark K, Urban JPG. Variation with age in the pattern of type X collagen expression in normal and scoliotic human intervertebral discs. *Calcified Tissue International*. Published online 1998. doi:10.1007/s002239900524

40. Weivoda MM, Youssef SJ, Oursler MJ. Sclerostin expression and functions beyond the osteocyte. *Bone*. Published online 2017. doi:10.1016/j.bone.2016.11.024

41. Tomlinson RE, Christiansen BA, Giannone AA, Genetos DC. The Role of Nerves in Skeletal Development, Adaptation, and Aging. *Frontiers in Endocrinology*. 2020;11. doi:10.3389/fendo.2020.00646

42. Ke HZ, Richards WG, Li X, Ominsky MS. Sclerostin and dickkopf-1 as therapeutic targets in bone diseases. *Endocrine Reviews*. Published online 2012. doi:10.1210/er.2011-1060

43. Beighton P, Durr L, Hamersma H. The clinical features of sclerosteosis. A review of the manifestations in twenty five affected individuals. *Annals of Internal Medicine*. 1976;84(4). doi:10.7326/0003-4819-84-4-393

44. Cardinal M, Chretien A, Roels T, et al. Gender-Related Impact of Sclerostin Antibody on Bone in the Osteogenesis Imperfecta Mouse. *Frontiers in Genetics*. 2021;12. doi:10.3389/fgene.2021.705505

45. Yee CS, Manilay JO, Chang JC, et al. Conditional Deletion of Sost in MSC-Derived Lineages Identifies Specific Cell-Type Contributions to Bone Mass and B-Cell Development. *Journal of Bone and Mineral Research*. 2018;33(10). doi:10.1002/jbmr.3467

Maier JA, Lo YT, Harfe BD. Foxa1 and Foxa2 Are Required for Formation of the Intervertebral Discs. *PLoS ONE*. Published online 2013. doi:10.1371/journal.pone.0055528

Bowles RD, Setton LA. Biomaterials for intervertebral disc regeneration and repair. *Biomaterials*. Published online 2017. doi:10.1016/j.biomaterials.2017.03.013

48 Vo N v., Hartman RA, Patil PR, et al. Molecular mechanisms of biological aging in intervertebral discs. *Journal of Orthopaedic Research*. Published online 2016. doi:10.1002/jor.23195

Duffy DJ, Millane RC, Frank U. A heat shock protein and Wnt signaling crosstalk during axial patterning and stem cell proliferation. *Developmental Biology*. Published online 2012. doi:10.1016/j.ydbio.2011.11.014

Chooi WH, Chan BP. Compression loading-induced stress responses in intervertebral disc cells encapsulated in 3D collagen constructs. *Scientific Reports*. Published online 2016. doi:10.1038/srep26449

51. Takao T, Iwaki T. A comparative study of localization of heat shock protein 27 and heat shock protein 72 in the developmental and degenerative intervertebral discs. *Spine*. Published online 2002. doi:10.1097/00007632-200202150-00007

52. Mundy C, Yasuda T, Kinumatsu T, et al. Synovial joint formation requires local Ext1 expression and heparan sulfate production in developing mouse embryo limbs and spine. *Developmental Biology*. Published online 2011. doi:10.1016/j.ydbio.2010.12.022

53. Hiyama A, Yokoyama K, Nukaga T, Sakai D, Mochida J. A complex interaction between Wnt signaling and TNF-α in nucleus pulposus cells. *Arthritis Research and Therapy*. Published online 2013. doi:10.1186/ar4379

54. Winkler T, Mahoney EJ, Sinner D, Wylie CC, Dahia CL. Wnt signaling activates Shh signaling in early postnatal intervertebral discs, and re-activates Shh signaling in old discs in the mouse. *PLoS ONE*. Published online 2014. doi:10.1371/journal.pone.0098444